Helicene Appended Benzothiadiazoles as Chiral Emitters

Kévin Martin, Tal Aharon, Maurizio Mastropasqua Talamo, Andreas Hauser, Thomas Bürgi, Nicolas Vanthuyne, Marco Caricato, Narcis Avarvari

Helicene Appended Benzothiadiazoles as Chiral Emitters

Kévin Martin,[a] Tal Aharon,[b,c] Maurizio Mastropasqua Talamo,[a] Andreas Hauser,[d] Thomas Bürgi,[d] Nicolas Vanthuyne,[e] Marco Caricato,*[b] and Narcis Avarvari*[a]

[a] *Dr. K. Martin, Dr. M. Mastropasqua Talamo, Dr. N. Avarvari*
Univ Angers, CNRS, MOLTECH-Anjou
SFR MATRIX, F-49000 Angers (France)
E-mail: narcis.avarvari@univ-angers.fr

[b] *Dr. T. Aharon, Prof. M. Caricato*
Department of Chemistry, University of Kansas
1567 Irving Hill Road, Lawrence, Kansas 66045 (United States of America)
E-mail: mcaricato@ku.edu

[c] *Dr. T. Aharon (current address)*
TetraScience, 294 Washington St, Boston, MA 02108 (United States of America)

[d] *Prof. A. Hauser, Prof. T. Bürgi*
Department of Physical Chemistry
University of Geneva
30 Quai Ernest Ansermet, CH-1211 Geneva (Switzerland)

[e] *Dr. N. Vanthuyne*
Aix Marseille Univ, CNRS, Centrale Marseille
UAR 1739, FSCM, Chiropole, Marseille (France)

Abstract

A homologous series of 4,7-bis(aryl) substituted benzothiadiazole (BTD) compounds, containing the helicenic derivatives bis([4]helicene), bis([5]helicene) and bis([6]helicene), have been prepared upon a double Suzuki coupling between 3,6-bis(pinacolyl-borane)-BTD and the corresponding bromo-aryl precursors. The single crystal X-ray structure of the bis([4]helicene) compound shows the existence of both helicities (*M*) and (*P*) on the same molecule. All the compounds of the series are highly emissive in solution, with quantum yields of the emission ranging from 50 to 91%. The enantiopure compounds (*M,M*) and (*P,P*) for the BTD-bis([6]helicene) have been prepared from the corresponding enantiopure 2-bromo-[6]helicene

precursors. Their chiroptical properties have been investigated in correlation with density functional theory (DFT) calculations, which allowed to confidently assign the absolute configuration of the helicene arms and to characterize the different electronic transitions, including the low energy charge transfer excitation from helicenes to BTD. The enantiomerically pure fluorophores (*M*,*M*)- and (*P*,*P*)-BTD-bis([6]helicene), which exist in solution as two main conformers, according to the DFT calculations, show CPL activity in solution, with g_{lum} factors of $\approx 1.7\times10^{-3}$ at λ_{em} = 525 nm, and also in the solid state, with g_{lum} factors of $\approx 1.2\times10^{-3}$ in spite of the strong decrease of the quantum efficiency.

Introduction

The strongly emitting 2,1,3-benzothiadiazole (BTD) unit[1,2] has been extensively used over the years in the field of organic electronics, in the composition of materials for organic and dye sensitized solar cells, [3–8] organic light-emitting diodes,[9–13] organic field-effect transistors,[14–17] but also as fluorescent probes[18] or polymeric thermometers.[19] Thanks to its electron acceptor character,[20] BTD has been used as well in donor-acceptor systems,[21–24] while the presence of sp^2 nitrogen atoms in the five-member thiadiazole ring makes it a valuable coordinating unit in an increasing number of functional ligands and derived metal complexes.[25–28] Nevertheless, when considering the excellent emissive properties of BTD derivatives it is rather surprising that the number of chiral representatives is relatively limited. Indeed, several BTD containing chiral polymers which provided chiral aggregates with enhanced chiroptical properties have been reported,[29–32] while even less examples of small molecules are known to date. The latter concern helicene units condensed with either one[33] or two[34,35] thiadiazole rings at one or both ends of the helical framework, respectively, or a BTD double aza-[5]helicene, only described as racemate because of the fluxional configuration.[36] Worth mentioning is that thiadiazole-[7]helicene and bis(thiadiazole)-[8]helicene were used with outstanding results in the chiral functionalization of hybrid electrodes for the electrochemical water splitting process[35,37] through the chirality induced spin selectivity (CISS) effect,[38,39] while bis(thiadiazole)-[7] and –[9]helicenes[34] have shown interesting circularly polarized luminescence (CPL) activity.[40,41] Molecular materials embedded with CPL activity[42] are gaining more and more interest in view of their possible use in various fields such as CP-OLEDs,[43,44] bio-responsive imaging,[45] or anti-counterfeiting applications.[46] In this respect, heterohelicenes stand among the most promising classes of small molecules with outstanding chiroptical properties and CPL activity.[47–50] In our previous study[33] it turned out that the emission of thiadiazole-[7]helicene, with fused thiadiazole and helicene units, was switched off as a result of an efficient intersystem crossing (ISC) mechanism from singlet to triplet excited states. Consequently, no CPL activity was measurable for this compound. The legitimate question that might therefore arise concerns the influence of the connectivity type, e.g. condensation *versus* covalent linking, between BTD and helicenes on the emission and CPL properties of the resulting compounds. We describe herein the synthesis and characterization of a series of BTD fluorophores containing two aromatic substituents, including the configurationally flexible [4] and [5]helicenes and configurationally stable [6]helicenes, in the 4 and 7 positions of the BTD ring. Single crystal X-ray characterization for

the bis([4]helicene) compound is reported, together with the photophysical properties of the entire series. The chiroptical properties, backed up by density functional theory (DFT) calculations, and CPL activity of the BTD-bis([6]helicene) derivatives have been investigated as well.

Results and discussion

Synthesis and characterization of 3,6-diaryl-benzothiadiazoles

Although the main target BTD compounds were those containing helicenic substituents (**4c**-**4e** in Scheme 1), we have prepared as well, for comparison purposes, the smaller non-helicenic congeners 4,7-bis(phenyl)-BTD **4a** and 4,7-bis(naphthyl)-BTD **4b** (Scheme 1). The connecting position of the polyaromatic units is always 2. The synthesis of all the compounds was performed through a double Suzuki-Miyaura coupling reaction[51,52] between the 4,7-bis(pinacolyl-borane)-BTD and the corresponding bromo-aryl precursor (Scheme 1, see also the SI, Figures S1-S8). Compounds **4a** and **4b** were previously prepared by the reversed strategy, *i.e.* double C–C Suzuki coupling between 3,6-dibromo-BTD and phenylboronic acid[53] and 2-naphthylboronic acid, respectively,[54] while both **4a** and the 1-naphthyl isomer of **4b** have been recently prepared by the same procedure[55] we have applied here. The single-crystal X-ray structure of **4a** was reported in the same study. The brominated precursors 2-Br-[4]helicene **1**,[56,57] 2-Br-[5]helicene **2**[58,59] and 2-Br-[6]helicene **3**[60,61] (Scheme 1) have been prepared according to published procedures (see details in the SI).

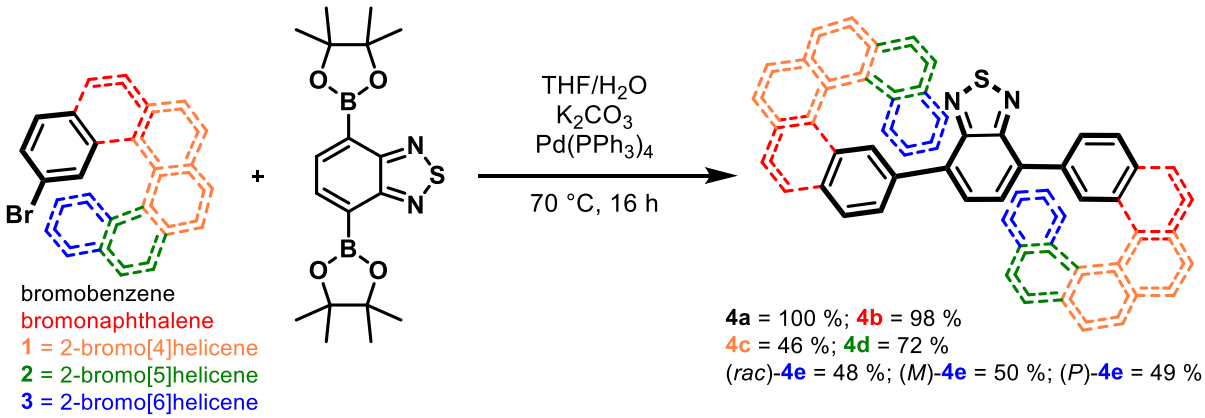

Scheme 1. Synthesis of 4,7-diaryl-benzothiadiazoles **4a-e**.

The enantiomerically pure compounds (*M*)-**4e** and (*P*)-**4e** have been obtained by using (*M*)- and (*P*)-2-bromo-[6]helicenes, respectively, which were separated by chiral HPLC from their racemic mixture.

The BTD **4a** afforded suitable single crystal for X-ray diffraction analysis upon slow evaporation of a solution of methylene chloride. It crystallized in the monoclinic space group $P2_1/c$, with one independent molecule in the asymmetric unit (see details in the SI, Figures S9-S11, Tables S1-S2). Dihedral angles of 34 and 42° are observed between the BTD core and the phenyl substituents which are twisted in the same direction. The structure we determined here slightly differs of the one very recently described,[55] where the single crystals were obtained in different conditions. Single crystals of the naphthyl derivative **4b** were obtained by the same procedure. The structure was solved in the monoclinic space group $P2_1/c$, with one independent molecule in the unit cell. The naphthyl substituents are twisted in opposite directions with respect to the BTD core, with dihedral angles of 55 and -45° (see structural details in the SI, Figures S12-S14, Tables S3-S4). Finally, we have succeeded to grow suitable single-crystals for X-ray analysis for the bis(helicenic) compound **4c** always by evaporation of a methylene chloride solution. The structure was solved in the monoclinic space group $P2_1/c$, with one independent molecule in the unit cell (see details in the SI, Figure S15, Tables S5-S6). Worth noting are the values of the dihedral angles between BTD and the helicene units, amounting at 35 and 28°, and the helical curvature (hc) of 30°, which expresses the dihedral angle between the first and the last benzene rings within a helicene. Moreover, one helicene has *M* conformation, while the other is *P*, and they are arranged in a mutual *trans* configuration with respect to the BTD core (Figure 1). Of course, in solution, the molecule should be highly fluxional because of the free rotation around the C–C single bonds and of the low enantiomerization barrier of the [4]helicene units.

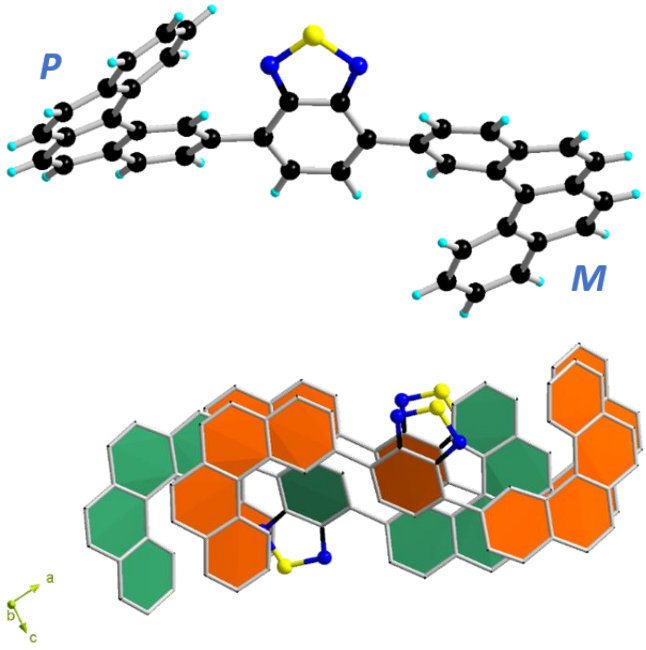

Figure 1. Molecular structure of BTD-bis([4]helicene) **4c** (top); view of the packing along the *b* axis (bottom).

The packing is driven by multiple π-π interactions between aromatic rings, the molecules are arranged in a head-to-tail fashion along the *b* direction (Figure 1, see also Figure S16), and the presence of the flanking helicene units hamper the establishment of the usual intermolecular N···S interactions typical for thiadiazoles.

Photophysical, chiroptical and theoretical study

The absorption spectra for the five compounds show similar features (Figure 2). Note the bathochromic shift of the low energy absorption band with the increasing number of fused aromatic rings, going from 380 (**4a**) to 415 nm (**4e**). This band corresponds to a charge transfer excitation from the aromatic substituents to the BTD unit.[33,55] A second absorption maximum is observed in the range 275 – 325 nm, also red-shifted from **4a** to **4e**. Upon excitation at 370 nm (**4a-b**) and 400 nm (**4c-e**), all the BTD compounds are emissive, with maxima at 475, 510, 533, 537 and 540 nm for **4a-e**, respectively (Figure 2).

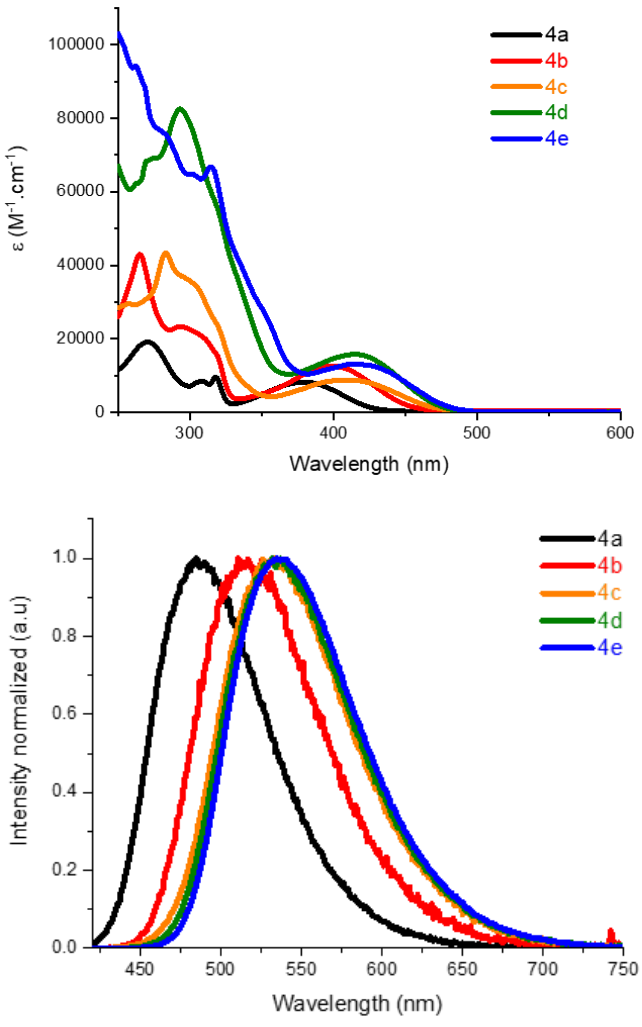

Figure 2. Absorption spectra of **4a-e** in CH_2Cl_2 solutions at room temperature; concentrations were in the range of 2 to $3x10^{-5}$ M (top). Emission spectra of **4a-e** in CH_2Cl_2 solutions at room temperature (bottom); for **4e** the (*M*,*M*) enantiomer is shown; concentrations were in the range of 2 to $3x10^{-5}$ M, the excitation wavelengths were 370 nm (**4a-b**) and 400 nm (**4c-e**), the spectra are corrected for the response function of the spectrometer and the intensities are normalised.

The value for **4a** corresponds to the one reported,[55] that for **4b** is red-shifted compared to its 1-naphthyl isomer, i.e. 490 nm,[55] showing the importance of the connecting position, while those for the helicene substituents are in the same range with the values for anthracenyl and pyrenyl substituents,[55] that is strongly red-shifted with respect to the first two as a consequence of the more extended π-system. The emission quantum efficiencies measured at room temperature in methylene chloride solutions, with $[Ru(bpy)_3]^{2+}$ as standard, indicate values of 90%, 82% and 77%, going from **4a** to **4c**. While the quantum yield for **4a** does correspond to the value recently reported,[55] the one for **4b** is clearly much higher than that of its 1-naphthyl isomer, announced at 27% in toluene solution,[55] measured with a different method though (integrating sphere). Then, the quantum efficiency of **4c** is slightly lower than the one for **4a**-**b**, possibly because of the fast inversion of the helical framework in [4]helicenes,[62,63] which makes **4c** somewhat more flexible than **4a** and **4b**. However, the values of the quantum yields determined for **4d** and **4e** are 60% and 51% respectively, upon measuring them with an integrating sphere, confirming the trend of a reduced radiative rate for the higher homologues of the series, very likely due to an efficient intersystem crossing.[33] Despite this monotonous decrease of the quantum yields of fluorescence when going from **4a** (90%) to **4e** (51%), the values are still of the same order of magnitude throughout the series. Note that the integration sphere was used for **4d** and **4e** in order to compare the emission in solution and in the solid state. Interestingly, the trend seems to be reversed in the solid state, where we observed a slightly increased quantum yield in the derivative **4e** compared to the **4d** with values of 12% and 8%, respectively. This could be ascribed to the bigger dimension of the [6]helicene systems that prevents slightly more efficiently (compared to [5]helicenes) the intermolecular π-π interactions around the BTD core causing the quenching of the fluorescence in the solid state.
The time dependent DFT (TD-DFT) absorption spectra of **4c**-**e** are blue-shifted overall by about 20 nm but are otherwise in good agreement with experimental spectra (see Figure S17 in the SI). Compared to the other two molecules, the **4c** peaks are slightly red shifted. The intensities for **4d** and **4e** are in good agreement with experimental spectra; however, the relative intensity compared to the other two molecules in the **4c** spectrum is nearly two times larger than in

experiment outside the 300-350 nm range. Fully matching all relative peak intensities would likely require more conformers for all three molecules, particularly **4c** (see discussion in the Computational Details section about the choice of conformers). Because there is an overall agreement in peak positions, we can use the simulated spectra for the peak assignment (peak wavelengths in the following text are taken from the calculated results). Each peak is a combination of multiple states, $\pi \rightarrow \pi^*$ in nature, where the electron density moves across the helicene arms through the central BTD unit, and *vice-versa*. More specifically, the transitions can be categorized in five common types. In every molecule, the first peak near 400 nm is always a HOMO → LUMO charge transfer, where the HOMO is spread out across the arms of the helicene and the benzene unit of the BTD, and the LUMO is entirely on the BTD unit (type 1). The second common type of transition is localized entirely on the helicene arms (type 2), and the third one is localized entirely on the BTD unit (type 3). The fourth common transition (4) comprises states where the electron density is initially spread across both helicene arms and moves to the central BTD unit. The final common transition (5) is a charge transfer from the central BTD unit to the helicene arms. The information about the transitions that form the simulated spectra are reported in Computational Section of the SI; the most important frontier molecular orbitals that contribute to these transitions are depicted in Figures S18-S23 of the SI. In the **4c** spectrum, there are peaks at 394, 320, 274, 259, and 237 nm. The 320 nm peak is a combination of type 2 and type 3 transitions, and the 274 nm peak is comprised of type 4 transitions. The 259 nm peak includes 2 transitions, and the 237 nm peak includes type 5 transitions. The peaks in the **4d** spectrum are at 392, 304, 274, and 250 nm. The 304 nm peak is a type 2 transition, while the 274 nm peak is a combination of type 5 and type 3 transitions, and the 250 nm peak are type 4 transitions. Finally, there are peaks at 391, 317, 266, and 243 nm in the **4e** spectrum. The 317 nm peak is characterized by type 4 transitions, the 266 nm peak also includes type 4 transitions, and the 243 nm peak is a type 5 transition.

Figure S17 in the SI presents calculated emission spectra for all three molecules, which are in good agreement in both peak positions and relative intensities. The peak maximum of the **4c** spectrum is correctly slightly blue shifted relative to the other two peaks, which are nearly on top of each other. All three transitions are $\pi^* \rightarrow \pi$ transitions (type 1).

Electronic and vibrational circular dichroism spectra have been measured for the two enantiomers (*M*,*M*) and (*P*,*P*) of **4e**, hereafter named (*M*)-**4e** and (*P*)-**4e** (Figure 3).

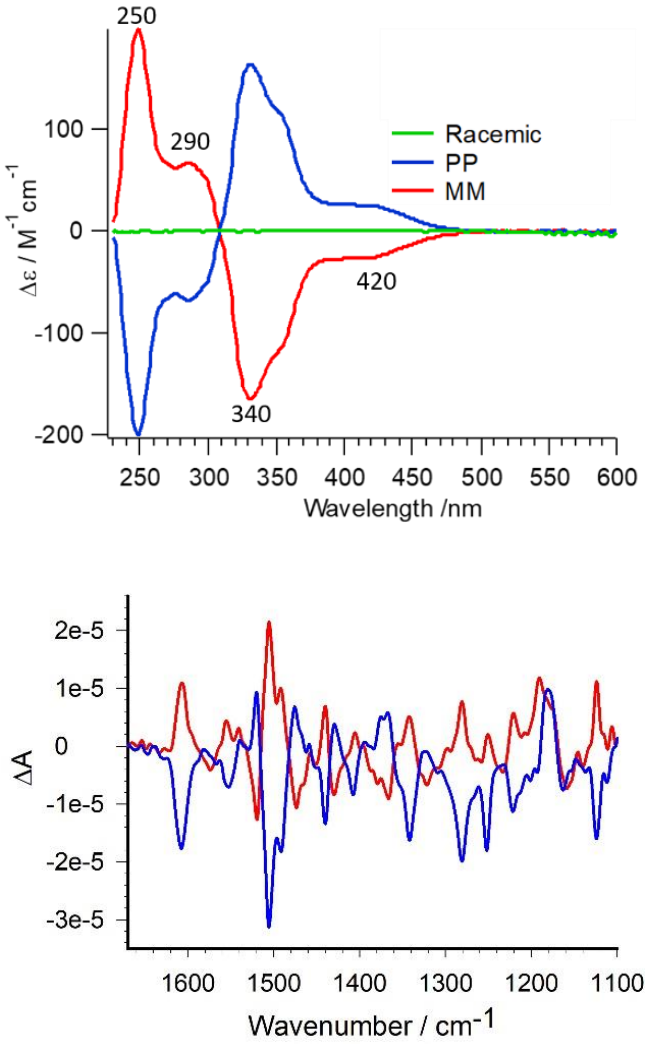

Figure 3. Experimental ECD spectra of **4e** in DCM (3×10^{-5} M) at room temperature (top); experimental VCD spectra of (*M*)-**4e** and (*P*)-**4e** for solutions of 4 mg in 150 µl $CDCl_3$ (path length: 0.2 mm, 14000 scans accumulation, a VCD spectrum of the solvent was subtracted in order to eliminate artefacts) (bottom).

As expected, no CD signal was detected for the racemic **4e**, which consists in fact of a mixture of (*M*)-**4e**, (*P*)-**4e** and (*M*,*P*)-**4e**, while the two enantiomers show mirror image spectra. In ECD, four bands are observed with maxima at 420, 340 (shoulder at 360), 290 and 250 nm, with that at low energy (420 nm) corresponding to the charge transfer excitation. The pattern for the three remaining bands at higher energies is typical for [6]helicenes, with a sequence –/–/+/+ (including the shoulder at 360 nm) for the rotatory strength of the (*M*) enantiomer.[64] Mirror image VCD spectra are also observed.

Because of the two C–C connections between the BTD core and the helicene units, one can infer that several conformers are in equilibrium in solution at room temperature for compound **4e**, and thus the experimental CD spectra would correspond to a Boltzmann population average of the most stable ones. As discussed in the Computational Details section, considering all

possible conformers with a larger basis set was unfeasible, and we concentrated on the two most stable ones, reported in Figure 4. Based on their relative energies, conformer **1** is more stable and accounts for 78% of the calculated spectra, while the other conformer **2** accounts for 22% of the spectra. However, the energy difference is overall small (less than 1 kcal/mol) and the electron density is fairly similar between the two.

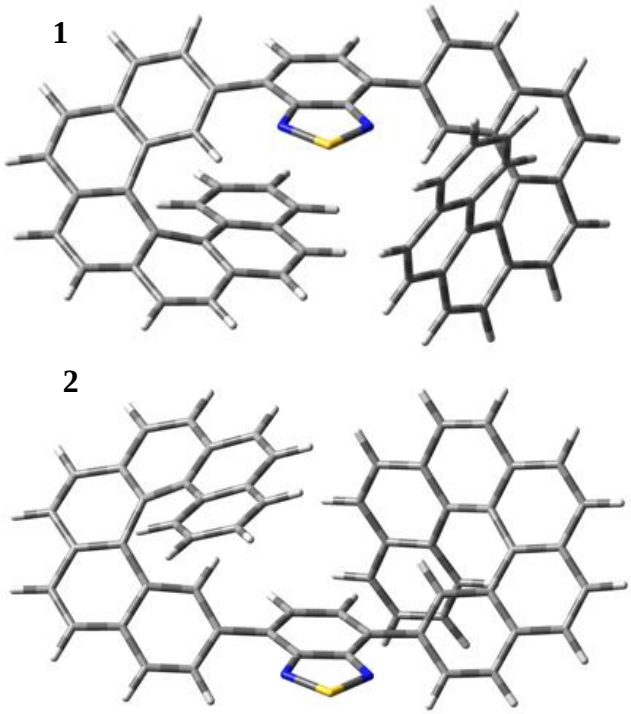

Figure 4. Relevant conformers of (*M*)-**4e,** optimized in CH_2Cl_2, and used in the simulated spectra. Conformer **1** (top) contributes with 78% of the spectra, and conformer **2** (bottom) with 22%.

The simulated ECD and VCD spectra for (*M*)-**4e** are presented in Figure 5. We find good agreement with the experimental ECD spectrum. The main peaks are at 393, 330, 287, and 238 nm. The negative peak at 250 nm is likely an artifact due to the limitations in the conformational sampling of the calculations. As mentioned above, the 393 nm peak is a type 1 transition, the 330 nm peak is a combination of type 2 and type 4 transitions, the 287 nm peak includes type 4 and type 5 transitions. The final peak at 238 nm is a combination of type 3, type 4, and transitions where electron density begins on both helicene arms and moves to a single arm. The simulated VCD spectrum is red-shifted by 61 cm^{-1} to align the large peak at about 1500 cm^{-1}. The calculation reproduces most of the main features of the experimental spectrum, including the negative peaks around the main positive 1500 cm^{-1} band, the positive peaks at 1339 cm^{-1} and 1262 cm^{-1} and the negative double-peak in between. Not all of the peaks are reproduced, for instance the positive band at 1600 cm^{-1}, and we attribute this to the limited conformational

sampling discussed above. Nonetheless, the agreement between the experimental and theoretical spectra further confirms the absolute configuration assignment for (*M*)-**4e** species (see also Figure S24).

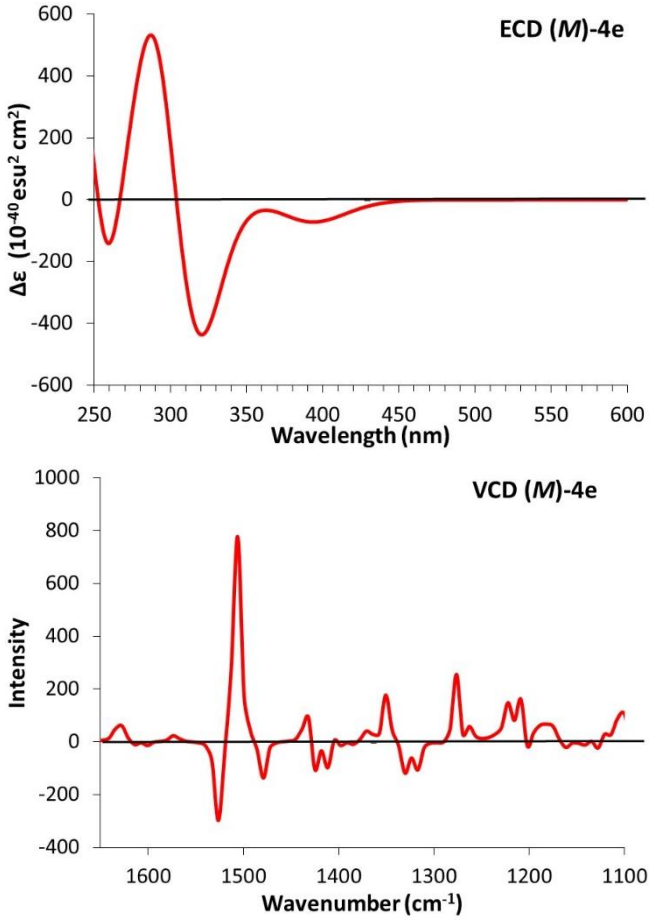

Figure 5. Simulated ECD (top) and VCD (bottom) spectra of (*M*)-**4e**.

Finally, the CPL activity of (*P*)-4e and (*M*)-4e was measured with a spectrometer conceived for Raman optical activity measurements[65] and previously used for other luminescent helicene derivatives.[66] The wavelength of the exciting radiation is 532 nm. The two enantiomeric chiral emitters show polarized luminescence with anisotropy factors $|g_{lum}|$ of $\approx 0.8\times10^{-3}$ at the maximum of emission (560 nm), in the normal range for organic small molecules, including helicenes.[49,50] The simulated CPL spectrum for (*M*)-**4e** is reported in Figure S25 of the SI and it is consistent with the experimental spectrum.

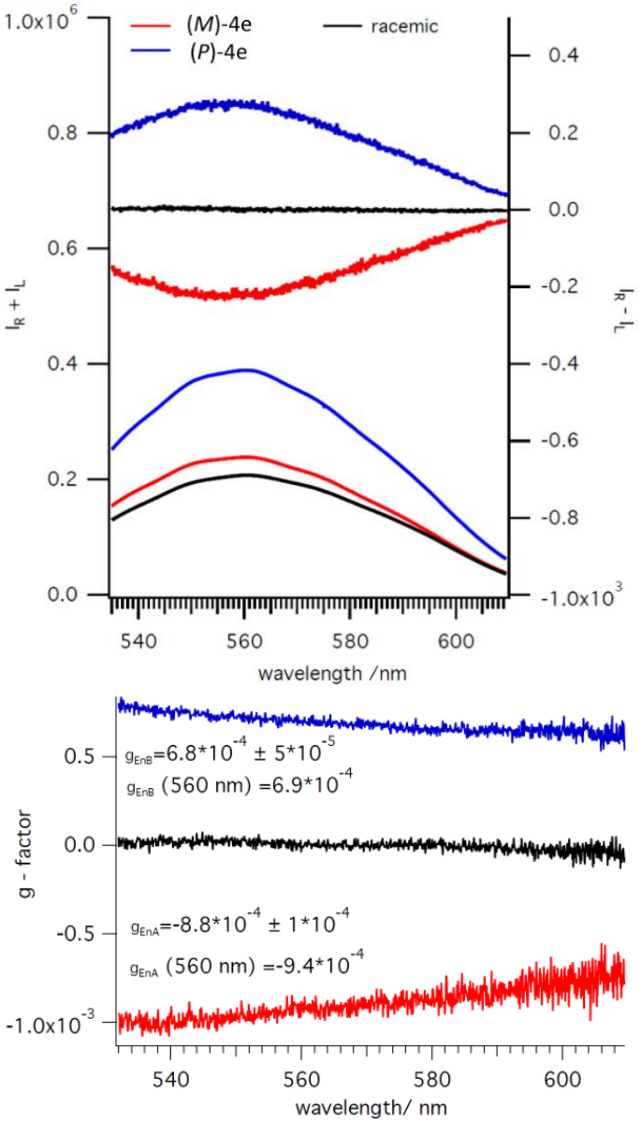

Figure 6. CPL spectra of (*P*)-**4e** (blue line) and (*M*)-**4e** (red line) (top) and anisotropy factors g_{lum} (bottom).

Alternatively, we have measured the CPL activity of **4e** with a JASCO CPL-300 spectrophotometer in solution and in the solid state (Figures S26-S27). The values in solution obtained by this classical method are only slightly higher, e.g. $|g_{lum}|$ of $\approx 1.7\times10^{-3}$, than those measured with the ROA equipment. Remarkably, the compound shows intense CPL activity in the solid state as well, i.e. $|g_{lum}|$ of $\approx 1.2\times10^{-3}$, in spite of the much lower quantum yield.

3. Conclusions

In this work we have reported first the straightforward synthesis of a homologous series of benzothiadiazole (BTD) fluorophores containing two covalently linked [4], [5] and [6]-helicenic units, i.e. compounds **4c**, **4d** and **4e**, respectively, together with their simpler non-helical bis(benzene) (**4a**) and bis(naphthalene) (**4b**) analogues. Single crystal X-ray diffraction

analysis of **4c** indicates the occurrence of the (*M*,*P*) diastereomer in the solid state. The bis([6]helicene) compound could be obtained as racemate but also as enantiopure derivatives (*M*,*M*) and (*P*,*P*) starting from the corresponding enantiopure 2-bromo-[6]helicene precursors. The photophysical study indicates strong emission of all BTD fluorophores, with quantum yields surpassing 50% in solution. The enantiopure BTD compounds have been chiroptically characterized by ECD and VCD. In the former, the lowest CD band corresponds to a charge transfer excitation from both helicene arms to the BTD ring and has negative sign for the (*M*,*M*) enantiomer, followed by the typical negative/positive couplet bands for (*M*) helicenes. The absolute configuration has been definitely attributed by measuring as well the VCD spectra of **4e** and confirmed by DFT calculations, an excellent agreement being observed between the Boltzmann averaged spectra and the experimental ones. Finally, compounds (*M*,*M*)-**4e** and (*P*,*P*)-**4e** showed CPL activity in solution, with anisotropy factors $|g_{lum}|$ reaching out 1.7×10^{-3} in solution (1.2×10^{-3} in the solid state) at the maximum of the emission, in accordance with the calculated CPL activity. It appears thus that the strategy of attaching covalently two configurationally stable helicene arms to BTD is relevant for the induction of CPL activity, with g_{lum} factors of the same order of magnitude with other molecular helicenic compounds, despite the fluxional nature of **4e** due to the free rotation around the connecting C–C bonds. These results open the way towards the use of configurationally stable BTD-bis(helicenes) as spin polarization materials through the CISS effect, the investigation of the helicene length on the CPL properties, or the attachment of two BTD units on a helicene platform in order to take advantage of the exciton coupling mechanism in the CPL activity. This research is under active investigation in our groups.

4. Experimental

4.1 Materials and methods

All reagents and chemicals from commercial sources were used without further purification. Solvents were dried and purified using standard techniques. Column chromatography was performed with analytical-grade solvents using Aldrich silica gel (technical grade, pore size 60 Å, 230-400 mesh particle size). Flexible plates ALUGRAM® Xtra SIL G UV254 from MACHEREY-NAGEL were used for TLC. Compounds were detected by UV irradiation (Bioblock Scientific) or staining with iodine, unless otherwise stated. NMR spectra were recorded with a Bruker AVANCE III 300 (^{1}H, 300 MHz and ^{13}C, 76 MHz, ^{19}F, 283 MHz, ^{31}P, 122 MHz) and Bruker AVANCE DRX 500 (^{1}H, 500 MHz and ^{13}C, 125 MHz). Chemical shifts

are given in ppm relative to tetramethylsilane TMS and coupling constants *J* in Hz. Residual non-deuterated solvent was used as an internal standard. UV-Vis absorption spectra were recorded at room temperature on a Perkin Elmer Lambda 950 spectrometer or with a Shimadzu UV-1800. Emission spectra were recorded on a PTI spectrofluorimeter mode, Quanta Master 1 coupled with a thermostat, using a Xenon lamp (70 W) as source and slits of 1 mm in a conventional quartz cell (light path 10 mm), or with a Shimadzu RF-6000. Matrix Assisted Laser Desorption/Ionization was performed on MALDI-TOF MS BIFLEX III Bruker Daltonics spectrometer using dithranol, DCTB or α-terthiophene as matrix. Circular dichroism (CD) measurements have been performed with a JASCO Corp. J-715 or J-810 apparatus. Chiral HPLC separation of (*rac*)-2-Br-[6]helicene was performed using a (*S*,*S*)-Whelk-O1 (250 x 10 mm) 5 µm column, with hexane / isopropanol / dichloromethane (83/2/15) as mobile phase.

4.2 Synthesis

General Procedure for Ar-BTD-Ar (4a-e): In a Schlenk tube under argon were dissolved the aryl bromide derivatives, i.e. bromo-benzene, 2-bromo-naphthalene and the 2-bromo-[n]helicenes (n = 4-6) **1-3** (3 eq), palladium tetrakis (5 mol%) and 4,7-bis(4,4,5,5-tetramethyl-1,3,2-dioxaborolan-2-yl)benzo[*c*][1,2,5]thiadiazole (1 eq) in 9.5 mL of THF. After degassing with argon for 10 min, a degassed solution of potassium carbonate (5 eq) in H_2O (1.5 mL) was added. The mixture was then stirred at 70 °C for 16 h. The dark green solution was allowed to reach the rt and 20 mL of CH_2Cl_2 were added. The organic layer was washed 3 times with water, 3 times with brine and then dried over $MgSO_4$. The crude product was concentrated under vacuum and then purified by column chromatography on silica gel (PE/DCM as eluent) to afford the desired compounds **4a-e**.

4,7-di(naphthalen-2-yl)benzo[c][1,2,5]thiadiazole (4b): General procedure from 2-bromo-naphthalene (160.1 mg, 773 µmol), $Pd(PPh_3)_4$ (14.9 mg, 13 µmol), 4,7-bis(4,4,5,5-tetramethyl-1,3,2-dioxaborolan-2-yl)benzo[*c*][1,2,5]thiadiazole (100 mg, 258 µmol), and K_2CO_3 (178.1 mg, 1.29 mmol). After purification (PE/DCM, 1/1, Rf = 0.73) compound **4b** was obtained as a yellow solid, 98 mg (98 % yield). Crystal suitable for X-ray analysis were obtained after slow evaporation in CH_2Cl_2.

^{1}H NMR (300 MHz, Chloroform-*d*) δ 8.51 (s, *J* = 1.6 Hz, 2H), 8.12 (dd, *J* = 8.5, 1.8 Hz, 2H), 8.03 (d, *J* = 9 Hz 3H), 8.01 – 7.96 (m, 3H), 7.95 – 7.92 (m, 2H), 7.57 – 7.54 (m, 4H).

^{13}C NMR (76 MHz, $CDCl_3$) δ 154.52, 135.01, 133.67, 133.54, 133.36, 128.82, 128.71, 128.66, 128.35, 127.87, 127.12, 126.69, 126.55.

MS (EI) m/z = 388.1037 **Calculated:** 388.1034.

4,7-bis(benzo[c]phenanthren-2-yl)benzo[c][1,2,5]thiadiazole (4c): General procedure from 2-bromo-[4]helicene (**1**) (237.5 mg, 773 µmol), $Pd(PPh_3)_4$ (14.9 mg, 13 µmol), 4,7-bis(4,4,5,5-tetramethyl-1,3,2-dioxaborolan-2-yl)benzo[*c*][1,2,5]thiadiazole (100 mg, 258 µmol), and K_2CO_3 (178.1 mg, 1.29 mmol). After purification (PE/DCM, 1/1, Rf = 0.82) compound **4c** was obtained as a yellow solid, 70 mg (46 % yield). Crystal suitable for X-ray analysis were obtained after slow evaporation in CH_2Cl_2.

^{1}H NMR (300 MHz, Chloroform-*d*) δ 9.90 (s, 2H), 9.54 (d, *J* = 8.5 Hz, 2H), 8.22 (s, 4H), 8.13, 8.04 (t, *J* = 7.5 Hz, 5H), 7.98 (d, *J* = 4.3 Hz, 2H), 7.94 (d, *J* = 5.4 Hz, 2H), 7.90 (s, 2H), 7.87 (s, 1H), 7.79 (t, *J* = 7.1 Hz, 2H), 7.66 (t, *J* = 7.6 Hz, 2H), 7.47 – 7.40 (m, 1H), 7.34 (t, *J* = 7.6 Hz, 1H).

^{13}C NMR (76 MHz, Chloroform-*d*) δ 155.66, 154.72, 154.57, 154.11, 139.59, 135.06, 134.96, 133.97, 133.72, 133.43, 133.27, 132.86, 131.48, 130.46, 129.63, 129.44, 129.01 – 128.37 (m), 127.90, 127.72, 127.56, 127.21, 126.96, 126.61, 126.44, 126.09.

MALDI-TOF = 588.1651 **Calculated** = 588.1660.

4,7-bis(dibenzo[c,g]phenanthren-9-yl)benzo[c][1,2,5]thiadiazole (4d): General procedure from 2-bromo-[5]helicene (**2**) (276.2 mg, 773 µmol), $Pd(PPh_3)_4$ (14.9 mg, 13 µmol), 4,7-bis(4,4,5,5-tetramethyl-1,3,2-dioxaborolan-2-yl)benzo[*c*][1,2,5]thiadiazole (100 mg, 258 µmol), and K_2CO_3 (178.1 mg, 1.29 mmol). After purification (PE/DCM, 6/4, Rf = 0.58) compound **4d** was obtained as an orange solid, 128 mg (72 % yield).

^{1}H NMR (300 MHz, Chloroform-*d*) δ 9.02 (d, *J* = 8.7 Hz, 2H), 8.75 (d, *J* = 8.4 Hz, 2H), 8.28 (m, 2H), 8.10 (d, *J* = 8.3 Hz, 2H), 8.07 – 8.04 (m, *J* = 7.7 Hz, 2H), 8.00 (s, 1H), 7.97 (t, *J* = 4.3 Hz, 3H), 7.95 (d, *J* = 3.2 Hz, 2H), 7.92 – 7.90 (m, 6H) 7.63 (t, *J* = 7.4 Hz, 2H), 7.52 (d, *J* = 3.7 Hz, 2H), 7.42 – 7.33 (m, 2H).

^{13}C NMR (126 MHz, Chloroform-*d*) δ 154.21, 133.77, 133.04, 132.73, 132.59, 132.52, 131.22, 129.76, 129.53, 129.42, 129.33, 129.12, 128.47, 128.25, 128.06, 127.74, 127.57, 127.49, 127.35, 127.26, 127.13, 126.59, 126.31, 124.97, 120.56.

MALDI-TOF = 688.1967 **Calculated** = 688.1973.

(*rac*+*meso*)-4,7-di(hexahelicen-11-yl)benzo[c][1,2,5]thiadiazole (4e): General procedure from (*rac*)-2-Br-bromo-[6]helicene (**3**) (157.4 mg, 386.5 µmol), $Pd(PPh_3)_4$ (7.44 mg, 6.4 µmol), 4,7-bis(4,4,5,5-tetramethyl-1,3,2-dioxaborolan-2-yl)benzo[*c*][1,2,5]thiadiazole (50 mg, 128.8

μmol), and K_2CO_3 (89 mg, 644 μmol). After purification (PE/DCM, 1/1, Rf = 0.6) compound **4e** was obtained as an orange solid, 49 mg (48 % yield).

^{1}H NMR (300 MHz, Chloroform-*d*) δ 8.16 (s, 2H), 8.06 – 7.98 (m, 19H), 7.93 – 7.89 (m, 2H), 7.86 – 7.78 (m, 4H), 7.30 (d, *J* = 7.0 Hz, 1H), 6.82 (t, *J* = 7.8 Hz, 2H), 6.43 (s, 2H).

^{13}C NMR (76 MHz, $CDCl_3$) δ 153.68, 134.50, 134.37, 133.47, 132.80, 132.41, 131.77, 131.67, 131.57, 130.32, 130.08, 130.03, 128.56, 128.38, 128.34, 128.04, 127.79, 127.71, 127.64, 127.57, 127.45, 127.29, 127.26, 126.99, 126.84, 126.12, 125.05, 124.99, 124.29.

MS (EI) m/z = 788.2286 **Calculated** = 788.2286.

(*M*,*M*)-4,7-di(hexahelicen-11-yl)benzo[c][1,2,5]thiadiazole ((*M*)-4e): General procedure from (*M*)-2-bromo-[6]helicene ***(M*-3**) (125.9 mg, 309.2 μmol), $Pd(PPh_3)_4$ (6 mg, 5.2 μmol), 4,7-bis(4,4,5,5-tetramethyl-1,3,2-dioxaborolan-2-yl)benzo[*c*][1,2,5]thiadiazole (40 mg, 103.1 μmol), and K_2CO_3 (71.2 mg, 515 μmol). After purification (PE/DCM, 1/1, Rf = 0.6) compound (*M*)-**4e** was obtained as an orange solid, 41 mg (50 % yield).

(*P*,*P*)-4,7-di(hexahelicen-11-yl)benzo[c][1,2,5]thiadiazole ((*P*)-4e): General procedure from (*P*)-2-bromo-[6]helicene ***(P*-3**) (157.4 mg, 386.5 μmol), $Pd(PPh_3)_4$ (7.44 mg, 6.4 μmol), 4,7-bis(4,4,5,5-tetramethyl-1,3,2-dioxaborolan-2-yl)benzo[*c*][1,2,5]thiadiazole (50 mg, 128.8 μmol), and K_2CO_3 (89 mg, 644 μmol). After purification (PE/DCM, 1/1, Rf = 0.6) compound (*P*)-**4e** was obtained as an orange solid, 40 mg (49 % yield).

4.3. X-Ray structure determinations

Details about data collection and solution refinement are given in Table SX. Single crystals of the compounds were mounted on glass fibre loops using a viscous hydrocarbon oil to coat the crystal and then transferred directly to cold nitrogen stream for data collection. Data collection were mostly performed at 150 K on an Agilent Supernova with CuKα (λ = 1.54184 Å). The structures were solved by direct methods with the SIR97 program and refined against all F_2 values with the SHELXL-97 program[67] using the WinGX graphical user interface.[68] All non-H atoms were refined anisotropically. Hydrogen atoms were introduced at calculated positions (riding model), included in structure factor calculations but not refined.

Deposition Number(s) <url href="https://www.ccdc.cam.ac.uk/services/structures?id=doi:10.1002/chem.202401413">2341523 (for **4a**), 2341524 (for **4b**), 2341525 (for **4c**)</url> contain(s) the supplementary crystallographic data for this paper. These data are provided free of charge by the joint

Cambridge Crystallographic Data Centre and Fachinformationszentrum Karlsruhe <url href="http://www.ccdc.cam.ac.uk/structures">Access Structures service</url>.

4.4 Vibrational circular dichroism

IR and vibrational circular dichroism (VCD) spectra were recorded on a Bruker PMA 50 accessory coupled to a Tensor 27 Fourier transform infrared spectrometer. A photoelastic modulator (Hinds PEM 90) set at l/4 retardation was used to modulate the handedness of the circular polarized light. Demodulation was performed by a lock-in amplifier (SR830 DSP). An optical low-pass filter (< 1800 cm^{-1}) in front of the photoelastic modulator was used to enhance the signal/noise ratio. Solutions of 4 mg/150 µl deuterated $CDCl_3$ were prepared and measured in a transmission cell equipped with CaF_2 windows and a 200 µm spacer. The VCD spectrum of the pure solvent served as the reference and was subtracted from the VCD spectrum of the compound in order to eliminate artefacts. For both the sample and the reference, ca. 14000 scans at 4 cm^{-1} resolution were averaged.

4.5 Computational details

All calculations were performed with a development version of the GAUSSIAN suite of programs.[69] Geometries were optimized using the CAM-B3LYP[70] model chemistry with D3 dispersion corrections.[71] Since these are conformationally flexible molecules, multiple minima are present, which need to be accounted for to reproduce the experimental spectra. We first determined all stable conformers at CAM-B3LYP/6-31G(d) level. We then selected enough conformers such that the total Boltzmann contribution was greater than 70% (2 conformers for each molecule), and re-optimized these structures with the aug-cc-pVDZ basis set. We computed the spectra for the selected conformers with the larger basis set, with Boltzmann weighting evaluated with the new energies. Thus, each plot is a population average of the individual spectra for each of the two major conformers. Calculations of absorption, ECD, and emission spectra were performed at the same level of theory (CAM-B3LYP/aug-cc-pVDZ) in the velocity gauge. Solvent effects were accounted for using the polarizable continuum model (PCM)[72–74] and the SMD radii.[75] The geometry optimizations, both in the ground and in the first excited state, were conducted in the equilibrium solvation regime, i.e., using the static dielectric constant of the solvent (ε=8.93 for DCM). The electronic transition calculations, both in absorption and emission, were performed in the non-equilibrium regime, where the solvent

electronic response was computed using the optical dielectric constant (ε_∞=2.0883 for DCM) while the nuclear and molecular solvent response was kept frozen at the equilibrium value.[74,76]

4.6 CPL measurements

CPL experiments described in this work were performed with the Raman optical activity (ROA) spectrometer designed by Hug and coworkers.[65,77] It is based on unique elements, *i.e.* a customized spectrograph and correction optics, which are designed to increase the signal - to-noise ratio and minimize artefacts. Briefly, the sample is excited with a continuous wave frequency doubled Nd:YAG laser. Emitted light is detected in backscattering configuration using a CCD camera (Wright Instruments) equipped with a CCD30-11-0-232 sensor. The laser is focused into the sample cell by a plano-convex lens with a focal length of 100 mm. Emitted light is collected by means of a gradium f/1.1 lens. Right (RCP) and left circular polarized (LCP) components in the signal beam are analysed using a liquid crystal retarder (LCR, Meadowlark Optics, Frederick Co, USA), which converts the two circular polarized components into linear polarized (LP) light with perpendicular planes of polarization. Using two polarization cubes the two perpendicular components (s- and p-branch) are split and transferred independently *via* optical fibers to a customized spectrograph (Kaiser Optical Systems). The light from the two fibers is coupled into the entrance slit of the spectrograph such that the s- and p-branch illuminate one half of the CCD camera. The spectrum is retrieved as the difference between the top and bottom half of the CCD. A dedicated corrections cycle is applied to eliminate artefacts as described in detail in ref. [77]. Alternatively, CPL measurements have been also performed in solution and in the solid state with a JASCO CPL-300 Circularly Polarized Luminescence Spectrophotometer (see the SI).

Conflicts of interest

There are no conflicts to declare.

Supporting Information

Additional references cited within the Supporting Information.[78–82]

Acknowledgements

This work was supported in France by the CNRS, the University of Angers and the RFI LUMOMAT (grant to K.M.). T.A. and M.C. gratefully acknowledge support from the National Science Foundation through Grant No. CHE-1650942.

Keywords

benzothiadiazole; chirality; circularly polarized luminescence; DFT calculations; helicenes

Notes and references

[1] B. A. D. Neto, A. A. M. Lapis, E. N. da Silva Júnior, J. Dupont, *Eur. J. Org. Chem.* **2013**, 228–255.

[2] N. S. Gudim, E. A. Knyazeva, L. V. Mikhalchenko, I. S. Golovanov, V. V. Popov, N. V. Obruchnikova, O. A. Rakitin, *Molecules* **2021**, *26*, 4931.

[3] M. Velusamy, K. R. J. Thomas, J. T. Lin, Y. Hsu, K. Ho, *Org. Lett.* **2005**, *7*, 1899–1902.

[4] Z.-M. Tang, T. Lei, K.-J. Jiang, Y.-L. Song, J. Pei, *Chem Asian J.* **2010**, *5*, 1911–1917.

[5] Y. Lin, Y. Li, X. Zhan, *Chem. Soc. Rev.* **2012**, *41*, 4245–4272.

[6] Y. Geng, F. Pop, C. Yi, N. Avarvari, M. Grätzel, S. Decurtins, S.-X. Liu, *New J. Chem.* **2014**, *38*, 3269–3274.

[7] S. Haid, M. Marszalek, A. Mishra, M. Wielopolski, J. Teuscher, J.-E. Moser, R. Humphry-Baker, S. M. Zakeeruddin, M. Grätzel, P. Bäuerle, *Adv. Funct. Mater.* **2012**, *22*, 1291–1302.

[8] J. Du, M. C. Biewer, M. C. Stefan, *J. Mater. Chem. A* **2016**, *4*, 15771–15787.

[9] C. T. Chen, *Chem. Mater.* **2004**, *16*, 4389–4400.

[10] I. Bala, R. A. Kumar Yadav, M. Devi, J. De, N. Singh, K. Kailasam, J. Jayakumar, J.-H. Jou, C.-H. Cheng, S. Kumar Pal, *J. Mater. Chem. C* **2020**, *8*, 17009–17015.

[11] L.-A. Lozano-Hernández, J. Cameron, C. J. Riggs, S. Reineke, P. J. Skabara, *ChemPhotoChem* **2023**, *7*, e202200256.

[12] A. Pathak, K. R. Justin Thomas, M. Singh, J.-H. Jou, *J. Org. Chem.* **2017**, *82*, 11512−11523.

[13] S. Li, K. Liu, X.-C. Feng, Z.-X. Li, Z.-Y. Zhang, B. Wang, M. Li, Y.-L. Bai, L. Cui, C. Li, *Nat. Commun.* **2022**, *13*, 2850.

[14] T. Kono, D. Kumaki, J. Nishida, T. Sakanoue, M. Kakita, H. Tada, S. Tokito, Y. Yamashita, *Chem. Mater.* **2007**, *19*, 1218–1220.

[15] M. Zhang, H. N. Tsao, W. Pisula, C. Yang, A. K. Mishra, K. Müllen, *J. Am. Chem. Soc.* **2007**, *129*, 3472–3473.

[16] Y. Geng, R. Pfattner, A. Campos, J. Hauser, V. Laukhin, J. Puigdollers, J. Veciana, M. Mas-Torrent, C. Rovira, S. Decurtins, S.-X. Liu, *Chem. Eur. J.* **2014**, *20*, 7136–7143.

[17] S. E. Ozturk, R. Isci, S. Faraji, B. Sütay, L. A. Majewski, T. Ozturk, *Eur. Polym. J.* **2023**, *191*, 112028.

[18] B. A. D. Neto, P. H. P. R. Carvalho, J. R. Correa, *Acc. Chem. Res.* **2015**, *48*, 1560−1569.

[19] S. Uchiyama, K. Kimura, C. Gota, K. Okabe, K. Kawamoto, N. Inada, T. Yoshihara, S. Tobita, *Chem. Eur. J.* **2012**, *18*, 9552–9563.

[20] K. R. J. Thomas, J. T. Lin, M. Velusamy, Y.-T. Tao, C.-H. Chuen, *Adv. Funct. Mater.* **2004**, *14*, 83–90.

[21] F. Pop, A. Amacher, N. Avarvari, J. Ding, L. M. Lawson Daku, A. Hauser, M. Koch, J. Hauser, S.-X. Liu, S. Decurtins, *Chem. Eur. J.* **2013**, *19*, 2504–2514.

[22] F. Pop, S. Seifert, J. Hankache, J. Ding, A. Hauser, N. Avarvari, *Org. Biomol. Chem.* **2015**, *13*, 1040–1047.

[23] F. Pop, N. Avarvari, *Chem. Commun.* **2016**, *52*, 7906–7927.

[24] Y. Wang, T. Michinobu, *J. Mater. Chem. C* **2016**, *4*, 6200–6214.

[25] T. S. Sukhikh, D. A. Bashirov, N. V. Kuratieva, A. I. Smolentsev, A. S. Bogomyakov, V. A. Burilov, A. R. Mustafina, A. V. Zibarev, S. N. Konchenko, *Dalton Trans.* **2015**, *44*, 5727–5734.

[26] T. Mocanu, N. Plyuta, T. Cauchy, M. Andruh, N. Avarvari, *Chemistry* **2021**, *3*, 269–287.

[27] X. Han, Q. Cheng, X. Meng, Z. Shao, K. Ma, D. Wei, J. Ding, H. Hou, *Chem. Commun.* **2017**, *53*, 10314–10317.

[28] N. Plyuta, S. Petrusenko, V. N. Kokozay, T. Cauchy, F. Lloret, M. Julve, J. Cano, N. Avarvari, *Dalton Trans.* **2022**, *51*, 4760–4771.

[29] H. S. Oh, H. Jee, A. Baev, M. T. Swihart, P. N. Prasad, *Adv. Funct. Mater.* **2012**, *22*, 5074–5080.

[30] H. Jee, H.-S. Oh, J. Lee, *Appl. Sci.* **2020**, *10*, 8740.

[31] A. Lapprand, N. Khiri, D. Fortin, S. Jugé, P. D. Harvey, *Inorg. Chem.* **2013**, *52*, 2361–2371.

[32] H. S. Oh, S. Liu, H. Jee, A. Baev, M. T. Swihart, P. N. Prasad, *J. Am. Chem. Soc.* **2010**, *132*, 17346–17348.

[33] T. Biet, K. Martin, J. Hankache, N. Hellou, A. Hauser, T. Bürgi, N. Vanthuyne, T. Aharon, M. Caricato, J. Crassous, N. Avarvari, *Chem. Eur. J.* **2017**, *23*, 437–446.

[34] Z. Zhang, Y. Murata, T. Hirose, *Tetrahedron* **2023**, *142*, 133514.

[35] Y. Liang, K. Banjac, K. Martin, N. Zigon, S. Lee, N. Vanthuyne, F. A. Garcés-Pineda, J. R. Galán-Mascarós, X. Hu, N. Avarvari, M. Lingenfelder, *Nat. Commun.* **2022**, *13*, 3356.

[36] Z. Yu, G. Shi, K.-P. Wang, L.-Z. Xu, S. Chen, Z.-Q. Hu, *Tetrahedron* **2023**, *130*, 133178.

[37] P. Vensaus, Y. Liang, N. Zigon, N. Avarvari, V. Mujica, G. Soler-Illia, M. Lingenfelder, *J. Chem. Phys.* **2024**, *160*, 111103.

[38] G. L. J. A. Rikken, N. Avarvari, *J. Phys. Chem. Lett.* **2023**, *14*, 9727–9731.

[39] B. P. Bloom, Y. Paltiel, R. Naaman, D. H. Waldeck, *Chem. Rev.* **2024**, *124*, 1950–1991.

[40] J. P. Riehl, F. S. Richardson, *Chem. Rev.* **1986**, *86*, 1–16.

[41] L. Arrico, L. Di Bari, F. Zinna, *Chem. Eur. J.* **2021**, *27*, 2920–2934.

[42] J. Han, S. Guo, H. Lu, S. Liu, Q. Zhao, W. Huang, *Adv. Optical Mater.* **2018**, *6*, 1800538.

[43] F. Zinna, U. Giovanella, L. Di Bari, *Adv. Mater.* **2015**, *27*, 1791–1795.

[44] J. R. Brandt, F. Salerno, M. J. Fuchter, *Nat. Rev. Chem.* **2017**, *1*, 0045.

[45] M. C. Heffern, L. M. Matosziuk, T. J. Meade, *Chem. Rev.* **2014**, *114*, 4496–4539.

[46] L. E. MacKenzie, R. Pal, *Nat. Rev. Chem.* **2021**, *5*, 109–124.

[47] Y. Yamamoto, H. Sakai, J. Yuasa, Y. Araki, T. Wada, T. Sakanoue, T. Takenobu, T. Kawai, T. Hasobe, *Chem. Eur. J.* **2016**, *22*, 4263–4273.

[48] T. Yanagi, T. Tanaka, H. Yorimitsu, *Chem. Sci.* **2021**, *12*, 2784–2793.

[49] K. Dhbaibi, L. Favereau, J. Crassous, *Chem. Rev.* **2019**, *119*, 8846–8853.

[50] F. Pop, N. Zigon, N. Avarvari, *Chem. Rev.* **2019**, *119*, 8435–8478.

[51] N. Miyaura, A. Suzuki, *J. Chem. Soc., Chem. Commun.* **1979**, 866–867.

[52] N. Miyaura, K. Yamada, A. Suzuki, *Tetrahedron Lett.* **1979**, *20*, 3437–3440.

[53] L. Wang, W. Huang, R. Li, D. Gehrig, P. W. M. Blom, K. Landfester, K. A. I. Zhang, *Angew. Chem. Int. Ed.* **2016**, *55*, 9783–9787.

[54] D. Taylor, T. Malcomson, A. Zhakeyev, S. Cheng, G. M. Rosair, J. Marques-Hueso, Z. Xu, M. J. Paterson, S. J. Dalgarno, F. Vilela, *Org. Chem. Front.* **2022**, *9*, 5473–5484.

[55] R. Liu, C. Zhou, Q. Ding, L. Qu, K. Wang, H. Tang, Y. Li, C. Yang, *Dyes Pigm.* **2023**, *219*, 111588.

[56] M. A. Brooks, L. T. Scott, *J. Am. Chem. Soc.* **1999**, *121*, 5444–5449.

[57] C. Wäckerlin, J. Li, A. Mairena, K. Martin, N. Avarvari, K.-H. Ernst, *Chem. Commun.* **2016**, *52*, 12694–12697.

[58] R. El Abed, B. Ben Hassine, J.-P. Genêt, M. Gorsane, A. Marinetti, *Eur. J. Org. Chem.* **2004**, 1517–1522.

[59] B. Irziqat, A. Cebrat, M. Baljozović, K. Martin, M. Parschau, N. Avarvari, K.-H. Ernst, *Chem. Eur. J.* **2021**, *27*, 13523–13526.

[60] M. Jakubec, T. Beránek, P. Jakubík, J. Sýkora, J. Žádný, V. Církva, J. Storch, *J. Org. Chem.* **2018**, *83*, 3607–3616.

[61] J. Voigt, K. Martin, E. Neziri, M. Baljozović, C. Wäckerlin, N. Avarvari, K.-H. Ernst, *Chem. Eur. J.* **2023**, *29*, e202300134.

[62] S. Grimme, S. D. Peyerimhoff, *Chem. Phys.* **1996**, *204*, 411–417.

[63] M. Srebro, N. Govind, W. A. de Jong, J. Autschbach, *J. Phys. Chem. A* **2011**, *115*, 10930–10949.

[64] A. Abhervé, M. Mastropasqua Talamo, N. Vanthuyne, F. Zinna, L. Di Bari, M. Grasser, B. Le Guennic, N. Avarvari, *Eur. J. Inorg. Chem.* **2022**, e202200010.

[65] W. Hug, G. Hangartner, *J. Raman Spectrosc*. **1999,** *30*, 841–852.

[66] T. Biet, T. Cauchy, Q. Sun, J. Ding, A. Hauser, P. Oulevey, T. Bürgi, D. Jacquemin, N. Vanthuyne, J. Crassous, N. Avarvari, *Chem. Commun.* **2017**, *53*, 9210–9213.

[67] G. M. Sheldrick, *Programs for the Refinement of Crystal Structures*, Göttingen, **1996**.

[68] L. Farrugia, *J. Appl. Crystallogr.* **1999**, *32*, 837.

[69] M. J. Frisch, G. W. Trucks, H. B. Schlegel, G. E. Scuseria, M. A. Robb, J. R. Cheeseman, G. Scalmani, V. Barone, B. Mennucci, G. A. Petersson, H. Nakatsuji, M. Caricato, X. Li, H. P. Hratchian, A. F. Izmaylov, J. Bloino, G. Zheng, J. L. Sonnenberg, M. Hada, M. Ehara, K. Toyota, R. Fukuda, J. Hasegawa, M. Ishida, T. Nakajima, Y. Honda, O. Kitao, H. Nakai, T. Vreven, J. A. Montgomery Jr., J. E. Peralta, F. Ogliaro, M. Bearpark, J. J. Heyd, E. Brothers, K. N. Kudin, V. N. Staroverov, T. Keith, R. Kobayashi, J. Normand, K. Raghavachari, A. Rendell, J. C. Burant, S. S. Iyengar, J. Tomasi, M. Cossi, N. Rega, J. M. Millam, M. Klene, J. E. Knox, J. B. Cross, V. Bakken, C. Adamo, J. Jaramillo, R. Gomperts, R. E. Stratmann, O. Yazyev, A. J. Austin, R. Cammi, C. Pomelli, J. W. Ochterski, R. L. Martin, K. Morokuma, V. G. Zakrzewski, G. A. Voth, P. Salvador, J. J. Dannenberg, S. Dapprich, P. V. Parandekar, N. J. Mayhall, A. D. Daniels, O. Farkas, J. B. Foresman, J. V. Ortiz, J. Cioslowski, and D. J. Fox, Gaussian Development Version, Revision H.09+, Gaussian, Inc., Wallingford, CT, 2010.

[70] T. Yanai, D. P. Tew, N. C. Handy, *Chem. Phys. Lett.* **2004**, *393*, 51–57.

[71] S. Grimme, J. Antony, S. Ehrlich, H. Krieg, *J. Chem. Phys.* **2010**, *132*, 154104.

[72] S. Miertuš, E. Scrocco, J. Tomasi, *Chem. Phys.* **1981**, *55*, 117.

[73] E. Cancès, B. Mennucci, J. Tomasi, *J. Chem. Phys.* **1997**, *107*, 3032–3041.

[74] J. Tomasi, B. Mennucci, R. Cammi, *Chem. Rev.* **2005**, *105*, 2999–3093.

[75] A. V. Marenich, C. J. Cramer, D. G. Truhlar, *J. Phys. Chem. B* **2009**, *113*, 6378–6396.

[76] M. Caricato, B. Mennucci, J. Tomasi, F. Ingrosso, R. Cammi, S. Corni, G. Scalmani, *J. Chem. Phys.* **2006**, *124*, 124520.

[77] J. Haesler, *Construction of a New Forward and Backward Scattering Raman Optical Activity Spectrometer and Graphical Analysis of Measured and Calculated Spectra for (R)-[$^2H_1$,$^2H_2$,$^2H_3$]-Neopentane*, Université de Fribourg, thèse no 1509, **2006**.

[78] W. Hua, Z. Liu, L. Duan, G. Dong, Y. Qiu, B. Zhang, D. Cui, X. Tao, N. Cheng, Y. Liu, *RSC Adv.* **2015**, *5*, 75–84.

[79] R. H. Martin, J. Moriau, N. Defay, *Tetrahedron* **1974**, *30*, 179–185.

[80] T. Matsushima, S. Kobayashi, S. Watanabe, *J. Org. Chem.* **2016**, *81*, 7799–7806.

[81] T. Biet, A. Fihey, T. Cauchy, N. Vanthuyne, C. Roussel, J. Crassous, N. Avarvari, *Chem. Eur. J.* **2013**, *19*, 13160–13167.

[82] J. Shen, R. Steinbach, J. M. Tobin, M. Mouro Nakata, M. Bower, M. R. S. McCoustra, H. Bridle, V. Arrighi, F. Vilela, *Appl. Catal., B* **2016**, *193*, 226–233.

Table of Contents Entry

Highly emissive covalently linked benzothiadiazole 4,7-bis(helicenes), with the [6]helicene representatives showing CPL activity in solution and in the solid state, have been obtained through a straightforward strategy.

Twitter: @MOLTECH_Anjou